Non-linear luminescent coupling in series-connected multijunction solar cells

Myles A. Steiner and John F. Geisz
National Renewable Energy Laboratory, Golden, Colorado 80401, USA

(Received 11 April 2012; accepted 4 June 2012; published online 21 June 2012)

The assumption of superposition or linearity of photocurrent with solar flux is widespread for calculations and measurements of solar cells. The well-known effect of luminescent coupling in multijunction solar cells has also been assumed to be linear with excess current. Here we show significant non-linearities in luminescent coupling in III-V multijunction solar cells and propose a simple model based on competition between radiative and nonradiative processes in the luminescent junction to explain these non-linearities. We demonstrate a technique for accurately measuring the junction photocurrents under a specified reference spectrum, that accounts for and quantifies luminescent coupling effects. © *2012 American Institute of Physics*.
[http://dx.doi.org/10.1063/1.4729827]

Radiative recombination is an unavoidable loss mechanism even in high-quality multijunction solar cells. Some fraction of the photogenerated electron-hole pairs will recombine in the active region and a fraction of those may luminesce at the bandedge, emitting photons up toward the front of the cell and down toward lower bandgap junctions in a multijunction device. The luminescent photons that are re-absorbed in the junction from which they were emitted effectively increase the radiative lifetime, thereby lowering the dark current and raising the open-circuit voltage,[1–3] a process known as photon recycling. The luminescent photons that are re-absorbed by a lower bandgap junction contribute to the photocurrent of that junction, a process known as luminescent coupling (LC).[4,5] In devices with good material quality, exemplified by many of the recent III-V triple-junction solar cells[6–9] that have achieved conversion efficiencies exceeding 40%, the radiative recombination rate may substantially exceed the non-radiative recombination rate, and the resulting luminescent coupling currents can significantly alter the junction photocurrents under a given reference spectrum.

The total electron-hole recombination rate depends on the operating point of the junction, which in a subcell of a multijunction device may differ from the conventional maximum power point. The net radiative recombination rate also depends on the geometry. Recombination is enhanced when a junction is driven into forward biases near the open-circuit voltage V_{oc}, where the quasi-Fermi-level gradients that are responsible for separating the photogenerated minority carriers are flattened, and the cross-section for carrier capture increases. At these voltages, a solar cell functions like a light emitting diode (LED). For a photon emitted in the bulk of the absorber layer, there is a probability of it being re-absorbed in the same layer, dependent on the emission energy, location and angle-integrated reflectances at the surrounding interfaces.[2,10,11] There is a related probability that the photon will be re-absorbed in a lower bandgap junction of a multijunction device, yielding a luminescent coupling current. This effect has been studied by looking at quantum efficiency (QE) measurements of a germanium photodiode with a GaInAs filtering layer,[12] as well as in QE measurements of multijunction cells.[13,14]

In this letter, we show evidence of a non-linear relationship between the luminescent coupling current and the excess recombination current, and propose a simple model based on the competition between radiative and non-radiative processes. The total short-circuit current of a series-connected, or tandem, multijunction solar cell (up to three junctions) is quantitatively explained in the presence of luminescent coupling. The presence of this non-linear luminescence current has profound implications for measurements of multijunction photovoltaic devices.

Consider first the physical situation illustrated in Fig. 1, for the subcells in a hypothetical two-junction device that is bottom-junction limited under the illuminating spectrum. The solid lines show the IV curves of each junction with their respective externally induced photocurrents, by which we mean the photocurrents induced by directly absorbed solar photons. Since the operating points of the various junctions are constrained by the requirement of current continuity

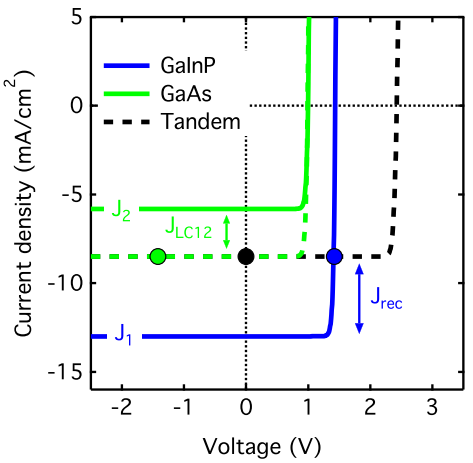

FIG. 1. Relative configuration of IV curves in a bottom-junction limited tandem. The large dots indicate the operating points when the device is at short-circuit. The dashed lines show the equilibrium IV curves of the bottom cell (green) and full device (black) in the presence of luminescent coupling.

through the device, the bottom junction operates in reverse bias when the overall device is biased at zero volts (short-circuit), whereas the top junction operates in forward bias near its V_{oc}. Strong luminescent coupling can occur with the IV curves in this configuration, with the magnitude of the coupling related to the recombination current in the upper cell.

Luminescence from the top junction adds to the photocurrent of the second junction, shifting the second junction IV curve down. This in turn shifts the operating point of the top junction downward and therefore reduces the recombination current, which then reduces the luminescence. An equilibrium is ultimately reached, shown by the green dashed line, which represents the actual bottom junction IV curve, including the luminescent coupling current, under the external solar spectrum that gave rise originally to the solid lines. The black dashed line is the equilibrium IV curve of the tandem. At equilibrium,

$$J_{\mathrm{LC12}} = \mathcal{L}_{12}(J_1 - [J_2 + J_{\mathrm{LC12}}]) \ , \tag{1}$$

where J_{LC12} is the current density resulting from luminescent coupling into the second junction, J_1 is the current density induced by the external illumination in the first (top) junction, and J_2 is the current density induced by the external illumination in the second junction. The argument of the function $\mathcal{L}$ represents the total recombination current in the top junction at equilibrium. We now derive a non-linear relationship to describe the observed behavior, using radiative and non-radiative components that may vary in relative magnitude as the total recombination current changes.

In the absence of series or shunting resistive elements and reverse-bias breakdown, the recombination current density for a pn junction can be described with a multi-diode model,

$$J_{\mathrm{rec}} = J_{01}\left(e^{\frac{qV}{kT}} - 1\right) + J_{0m}\left(e^{\frac{qV}{mkT}} - 1\right) + J_{0a}\left(e^{\frac{3qV}{2kT}} - 1\right), \tag{2}$$

where J_{01}, J_{0m}, and J_{0a} are the reverse saturation current densities of various recombination processes. The first, $m = 1$ term describes recombination in the quasi-neutral regions under low-injection conditions, which include both band-to-band radiative processes and non-radiative processes. The second, $m > 1$ term is characteristic of various non-radiative recombination mechanisms. To an excellent approximation,[15] the predominant non-radiative mechanism of Shockley-Read-Hall (SRH) recombination in the depletion region and near the perimeter is described by $m \sim 2$ for recombination through midgap states. $m = 2$ can also describe radiative recombination under high injection conditions. The third, $m = 2/3$ term describes Auger recombination.[16] Auger is not typically a dominant recombination mechanism in these III-V alloys with doping levels below $<10^{19}\,\mathrm{cm}^{-3}$ but is included for completeness.

The photon flux emitted by a higher bandgap upper junction i and re-absorbed by a lower junction j that gives rise to an LC current is a fraction of the first term of Eq. (2)

$$J_{\mathrm{LC}ij} = \eta_{ij} J_{01}\left(e^{\frac{qV}{kT}} - 1\right), \tag{3}$$

where η_{ij} is a coupling efficiency, constrained to be $0 \le \eta_{ij} \le 1$, that includes optical effects in the cell as well as the ratio between radiative and non-radiative recombination in the $m = 1$ term. The voltage dependence is explicitly described by the exponential. In forward bias, the -1 terms are relatively small and can be neglected; this assumption is good to very low recombination currents, so long as $J_{\mathrm{rec}} \gg J_{01},\ J_{0m},\ J_{0a}$. Combining Eqs. (2) and (3), we find

$$J_{\mathrm{rec}} = \frac{J_{\mathrm{LC}ij}}{\eta_{ij}} + J_{0m}\left(\frac{J_{\mathrm{LC}ij}}{\eta_{ij} J_{01}}\right)^{\frac{1}{m}} + J_{0a}\left(\frac{J_{\mathrm{LC}ij}}{\eta_{ij} J_{01}}\right)^{\frac{3}{2}}. \tag{4}$$

In general this equation can only be solved numerically for $J_{\mathrm{LC}ij}$, but for the most common case where the ideality factor $m = 2$ in the second diode term, it can be solved analytically as a cubic in $\sqrt{J_{\mathrm{LC}ij}/\eta_{ij}}$. Finally, when the Auger term can be neglected, a very simple analytical solution can be found:

$$J_{\mathrm{LC}ij} = \mathcal{L}_{ij}(J_{\mathrm{rec}}) = \eta_{ij}\left[\sqrt{\varphi_i^2 + J_{\mathrm{rec}}} - \varphi_i\right]^2, \tag{5}$$

where $\varphi_i = \frac{J_{02}}{2\sqrt{J_{01}}}$ is a property of the light-emitting upper junction i. Previous treatments of luminescent coupling have assumed a linearized functional form $J_{\mathrm{LC}} = \eta J_{\mathrm{rec}}$. This is indeed the limiting case of Eq. (5) where non-radiative SRH recombination is negligible and $\varphi_i \to 0$. An interesting difference between these functional forms, however, is that the derivative $dJ_{\mathrm{LC}ij}/dJ_{\mathrm{rec}}$ at $J_{\mathrm{rec}} = 0$ is η_{ij} for the linear model, but zero whenever $\varphi_i > 0$ in the non-linear expression. The $m > 1$ term gives rise to *superlinear* behavior, while the Auger term gives rise to *sublinear* behavior. As we will show, the III-V luminescent materials GaAs and GaInP appear to follow a superlinear behavior over the range of currents investigated in this study.

Equation (5) is still implicit because the recombination current itself depends on $J_{\mathrm{LC}ij}$. When the second junction of a multijunction cell (with an arbitrary total number of junctions) is limiting, $J_{\mathrm{rec}} = J_1 - J_2 - J_{\mathrm{LC12}}$, as described in Eq. (1). Substituting this expression into Eq. (5) and solving for J_{LC12} yields

$$J_{\mathrm{LC12}} = \frac{\eta_{12}}{(1+\eta_{12})^2}\left[\sqrt{\varphi_1^2 + (1+\eta_{12})\cdot(J_1 - J_2)} - \varphi_1\right]^2, \tag{6}$$

which is now explicitly dependent on the externally induced photocurrents.

In the case of a third-junction limited triple junction, the analysis proceeds similarly. The three externally induced photocurrents are denoted J_1, J_2, and J_3, from top to bottom, respectively. The operating points of the forward-biased middle and top junctions are determined by the total photocurrent in the third junction. In this case there can be three luminescent currents,

$$J_{\mathrm{LC12}} = \mathcal{L}_{12}(J_1 - J_3 - J_{\mathrm{LC23}} - J_{\mathrm{LC13}}) \tag{7a}$$

$$J_{\mathrm{LC13}} = \mathcal{L}_{13}(J_1 - J_3 - J_{\mathrm{LC23}} - J_{\mathrm{LC13}}) \tag{7b}$$

$$J_{\mathrm{LC23}} = \mathcal{L}_{23}(J_2 - J_3 + J_{\mathrm{LC12}} - J_{\mathrm{LC23}} - J_{\mathrm{LC13}}). \tag{7c}$$

The middle junction is typically optically thick at the wavelength of the top junction bandedge luminescence so that we can neglect J_{LC13}. Substituting Eq. (7a) into Eq. (7c), we find

$$J_{LC23} = \mathcal{L}_{23}\Big(J_2 - J_3 - J_{LC23} + \mathcal{L}_{12}(J_1 - J_3 - J_{LC23})\Big), \tag{8}$$

and using Eq. (5) this becomes

$$J_{LC23} = \eta_{23}\left[\sqrt{\varphi_2^2 + J_2 - J_3 - J_{LC23} + \eta_{12}\left[\sqrt{\varphi_1^2 + J_1 - J_3 - J_{LC23}} - \varphi_1\right]^2} - \varphi_2\right]^2. \tag{9}$$

The parameters η_{12} and φ_1 characterize the luminescence from the first to the second junction and η_{23} and φ_2 characterize the luminescence from the second to the third junction. Equation (9) can be reduced to a fourth-order polynomial in $\sqrt{J_{LC23}}$ and solved numerically.

As a result of luminescent coupling, accurate measurement of a particular junction's photocurrent cannot be accomplished by simply over-illuminating the remaining junctions and observing the resulting IV curve.[17] The amount of internal luminescence varies with the separation in externally induced photocurrents, and therefore is directly affected by the degree of over-illumination.

The total short-circuit current through a triple-junction device, under any spectrum, is limited to the minimum junction photocurrent

$$J_{sc} = \min\begin{cases} J_1 & \text{(10a)} \\ J_2 + J_{LC12} & \text{(10b)} \\ J_3 + J_{LC23} + J_{LC13} & \text{(10c)} \end{cases}$$

for top-, middle- and bottom-limited conditions, with J_{LC12} and J_{LC23} given by Eqs. (6) and (9), respectively, and J_{LC13} is again typically neglected. If we re-express the photocurrents J_1, J_2, and J_3 in terms of their values relative to one-sun, as $X_1 J_1^{1sun}, \ldots,$ etc., then the quantities (X_1, X_2, X_3) become the independent variables in Eq. (10). If the relative intensities are sequentially varied and measured, the total short-circuit current can be fit and the one-sun externally induced junction photocurrents extracted.

Figure 2 shows data collected at 25 °C for a GaInP/GaAs/GaInAs triple-junction solar cell with bandgaps 1.81/1.40/1.07 eV. Details about the cell fabrication can be found elsewhere.[6] IV measurements were taken on a class A solar simulator with a white-light xenon lamp and high-brightness LEDs with wavelengths 470, 850, and 940 nm. For every data point, the intensity on each junction relative to the ASTM G173 direct solar spectrum was determined by measuring the photocurrent on a corresponding calibrated single-junction reference cell, and correcting for any spectral mismatch using the measured instrument spectra.[18] The relative intensity of each junction was characterized as each LED was varied to account for any spectral overlap between the LEDs. The data show how the tandem J_{sc} changes as each of the LED intensities is varied. For the blue curves, the 470 nm LED was varied and the data are plotted as a function of the relative intensity on the top junction. For the green curves, the 850 nm LED intensity was varied and the data are plotted as a function of the relative intensity on the middle junction, and so on.

In Fig. 2(a), the white light was turned off and only LED light illuminated the sample. For the upper blue curve in Fig. 2(a), 470 nm light was varied and a constant background intensity of 940 nm light was added to over-illuminate the bottom junction, which effectively reduces the determination of J_{sc} to a two-junction problem. J_{sc} results in

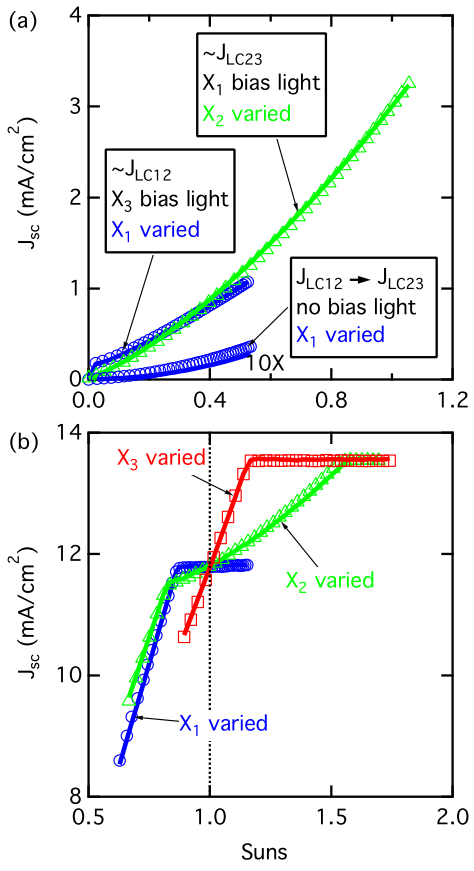

FIG. 2. Tandem J_{sc} for a triple junction, with varying LED light intensity. The horizontal axis is always the relative intensity on the junction corresponding to the varying LED (blue = X_1, green = X_2, red = X_3). (a) Data taken with only LED illumination. (b) Data taken around one-sun illumination. The solid lines are a simultaneous fit to Eq. (10). The fit parameters are found to be $J_1^{1sun} = 13.60$ mA/cm^2, $J_2^{1sun} = 13.72$ mA/cm^2, $J_3^{1sun} = 11.70$ mA/cm^2, $\eta_{12} = 0.240$, $\eta_{23} = 0.888$, $\varphi_{12} = 0.641$, and $\varphi_{23} = 3.271$.

this case mostly from the luminescent coupling current J_{LC12} from top to middle junctions, with a very small amount of direct illumination on the middle junction due to the spectral width of the two LEDs. The data directly demonstrate the functional dependence of Eq. (6). For the lower blue curve, 470 nm LED light was varied but with no additional bias light, and therefore J_{sc} results from the cascading luminescence $J_{LC12} \rightarrow J_{LC23}$. The curve is magnified by a factor of 10 for clarity and shows the functional dependence of Eq. (9). For the green curve, 850 nm light was varied and a constant background intensity of 470 nm light was added to over-illuminate the top junction, and J_{sc} results from J_{LC23} plus some LED spectral overlap. As we noted above, the derivative of all three curves approaches zero at the origin, and a linear model is clearly inappropriate.

In Fig. 2(b), the simulator was first adjusted to represent the one-sun reference spectrum using adjusted quantum efficiencies[19] and calibrated reference cells. The illumination included both white light and LED light so that the relative intensity on each junction could be increased or decreased. The LEDs were then sequentially varied around the one-sun illumination, with the relative intensity on each junction again measured at each point. In each curve, at low intensities J_{sc} is limited by the junction corresponding to the varying LED, but at some relative intensity becomes limited by a different junction. In the case of the green curve, for example, the device is middle-junction limited with low intensity 850 nm light, but then becomes bottom-junction limited at $X_2 \sim 0.83$. As the 850 nm LED intensity increases further, the middle junction luminescence J_{LC23} gradually increases, giving rise to the observed curvature, and at $X_2 \sim 1.6$, J_{LC23} becomes sufficiently large that the total bottom junction photocurrent $J_3 + J_{LC23}$ exceeds even J_1. The device is thereafter top-junction limited at the far-right of the graph.

The solid lines in Fig. 2 show a simultaneous fit of Eq. (10) to all of the data, with the fit parameters listed in the caption. Including the one-sun externally induced photocurrents, Eq. (10) has seven fitting parameters, and not all of the individual measurements are sensitive to every parameter. A unique solution can be found, however, providing that data are acquired over a sufficient range of limiting conditions so that there is sensitivity to each parameter, which generally requires the six measurements shown. As with any fitting routine, appropriate initial guesses for each parameter are essential. The one-sun values $J_1^{1\text{sun}}, \ldots,$ etc. can be estimated by integrating the quantum efficiency over the reference spectrum. η and φ depend on the material quality and geometry and are constrained to $0 \leq \eta \leq 1$ and $\varphi \geq 0$. In this way, we are able to unambiguously measure the externally induced photocurrents $J_1^{1\text{sun}}$, $J_2^{1\text{sun}}$, and $J_3^{1\text{sun}}$ under a particular reference spectrum.

The significance of the η parameters can be understood from optical modeling. As noted above, η represents the asymptotic value of the coupling efficiency in the limit $\varphi \rightarrow 0$. In general the modeling is complicated, accounting for all reflections and transmissions, re-absorption in the active layer, and integrating over the cell thickness, the solid angle, and the emission energy.[10] However, we can estimate an upper bound on η based on a simpler physical model. In the radiative limit, any photon emitted in a cell must eventually escape the junction through one of the two boundaries; if the photon strikes the boundary at a greater angle than the critical angle, it will be totally internally reflected and eventually re-absorbed, but we continue to follow its reincarnation as an electron-hole pair that will radiatively recombine along a different trajectory, and so on, until the photon strikes the boundary at a steep enough angle to escape. At the upper and lower boundaries, the angle-integrated transmittances T_U and T_L, and the reflectance R_L, are calculated using the algorithm of Bader *et al.*[20] based on the nominal thicknesses and dielectric data for the III-V alloys that make up the layers (e.g., tunnel junctions, confinement layers etc.). Including the absorption in the lower boundary layer, the maximum transmission probability $P_{\max}$ into the lower junction is

$$P_{\max} = \frac{T_L}{T_U + T_L}(R_L + T_L). \tag{11}$$

For the cell in Fig. 2, we calculate $P_{\max} = 0.87$ for the GaAs junction and $P_{\max} = 0.70$ for the GaInP junction. Comparing these values to the fit parameters, the GaAs junction $\eta_{23} \sim P_{\max}$, and the GaInP junction $\eta_{12} \sim \frac{1}{3} P_{\max}$. These are both reasonable values given the expected material quality of each junction and the modest uncertainty in the calculation.

The fit values of φ_1 and φ_2 can be compared with typical values for the coefficients J_{01} and J_{02}. For GaAs, J_{01} is in the range of 10^{-18}–10^{-17} mA/cm^2 and $J_{02} \sim 10^{-9}$–10^{-8} mA/cm^2, and we expect φ_2 to be of order 0.15–5. For GaInP, $J_{01} \sim 10^{-23}$–10^{-22} mA/cm^2 and $J_{02} \sim 10^{-11}$–10^{-10} mA/cm^2, and we expect φ_1 to be of order 0.5–10. Both estimates agree with the fit parameters.

An important consequence of Eq. (5) is that the typically assumed linearity of the short-circuit current with illumination intensity can be incorrect. For terrestrial applications, III-V multijunction solar cells are designed to operate under illumination intensities approaching 1000×, achieved by concentrating the incident light by means of a Fresnel lens or a parabolic mirror, for example. The externally induced photocurrents J_1, J_2, and J_3 are presumed to increase linearly as the overall concentration increases (assuming no chromatic aberration effects) but for a middle- or bottom-limited device the preceding analysis leads to the conclusion that the recombination currents in the non-limiting junctions increase non-linearly as J_1, J_2, and J_3 separate. This has implications for the measurement of triple-junction solar cells under high-intensity, low-injection conditions. The efficiency ε of a solar cell is determined by

$$\varepsilon = \frac{V_{oc} FF}{100}\left(\frac{J_{sc}}{X}\right), \tag{12}$$

where FF is the fill factor, X is the geometric concentration, and the irradiance at one-sun is 100 mW/cm^2. While the linear model for luminescent coupling results in a constant value of the ratio J_{sc}/X, the non-linear model presented here predicts an increase of 7.4% in the J_{sc}/X ratio at 1000 suns, using the fit parameters from Fig. 2. In a measurement of this particular solar cell at 1000× *assuming* linearity of

concentration with photocurrent, the actual concentration would be only 931 suns, and the efficiency would be underestimated by 7.4%. This is an extreme case, as the device was intentionally severely bottom-junction limited. Top-junction limited devices should remain linear since luminescent coupling does not contribute to its short-circuit current. For both middle- or bottom-limited devices, however, J_{sc} is predicted to increase super-linearly with concentration in the presence of luminescent coupling, unless there is no non-radiative recombination at all. If Auger recombination becomes important at high concentration, the super-linear behavior may roll over to become sub-linear.

We conclude by observing that strong luminescent coupling may or may not be advantageous in actual devices. Strong coupling is indicative of high quality material with low non-radiative losses, but complicates the measurements. It may buffer against current loss that results from current mismatch as the spectrum varies during the course of the day or year and therefore increase the total integrated energy yield.[21] If the photons were instead recycled within the emitting junction, an even higher energy yield may result.

It is a pleasure to thank NREL colleagues S. Kurtz, D. Friedman, J. Olson, B. McMahon, R. France, I. García, K. Emery, and T. Moriarty for useful conversations. Solar cells were fabricated by W. Olavarria, M. Young, and A. Duda. Research was supported by the U.S. Department of Energy under Contract No. DE-AC36-08GO28308 with the National Renewable Energy Laboratory. This work is subject to government rights.

[1]A. Marti, J. L. Balenzategui and R. F. Reyna, J. Appl. Phys. **82**, 4067 (1997).
[2]P. Asbeck, J. Appl. Phys. **48**, 820 (1977).
[3]E. Yablonovitch, T. J. Gmitter, and R. Bhat, Phys. Rev. Lett. **61**, 2546 (1988).
[4]C. H. Henry, J. Appl. Phys. **51**, 4494 (1980).
[5]A. Marti and G. L. Araujo, Sol. Energy Mater. Sol. Cells **43**, 203 (1996).
[6]J. F. Geisz, S. R. Kurtz, M. W. Wanlass, J. S. Ward, A. Duda, D. J. Friedman, J. M. Olson, W. E. McMahon, T. Moriarty, and J. Kiehl, Appl. Phys. Lett. **91**, 023502 (2007).
[7]J. F. Geisz, D. J. Friedman, J. S. Ward, A. Duda, W. J. Olavarria, T. E. Moriarty, J. T. Kiehl, M. J. Romero, A. G. Norman, and K. M. Jones, Appl. Phys. Lett. **93**, 123505 (2008).
[8]R. R. King, D. C. Law, K. M. Edmondson, C. M. Fetzer, G. S. Kinsey, H. Yoon, R. A. Sherif, and N. H. Karam, Appl. Phys. Lett. **90**, 183516 (2007).
[9]W. Guter, J. Schöne, S. P. Philipps, M. Steiner, G. Siefer, A. Wekkeli, E. Welser, E. Oliva, A. W. Bett, and F. Dimroth, Appl. Phys. Lett. **94**, 223504 (2009).
[10]J. L. Balenzategui and A. Marti, Sol. Energy Mater. Sol. Cells **90**, 1068 (2006).
[11]M. P. Patkar, M. S. Lundstrom, and M. R. Melloch, J. Appl. Phys. **78**, 2817 (1995).
[12]C. Baur, M. Hermie, F. Dimroth, and A. W. Bett, Appl. Phys. Lett. **90**, 192109 (2007).
[13]S. H. Lim, J.-J. Li, E. H. Steenbergen, and Y.-H. Zhang, "Luminescence coupling effects on multijunction solar cell external quantum efficiency measurement," Prog. Photovoltaics (to be published).
[14]M. A. Steiner, S. R. Kurtz, J. F. Geisz, W. E. McMahon, and J. M. Olson, "Using phase effects to understand measurements of the quantum efficiency and related luminescent coupling in a multijunction solar cell," J. Photovoltaics (to be published).
[15]J. Nelson, *The Physics of Solar Cells* (Imperial College, London, 2003).
[16]H. J. Queisse and M. B. Panish, J. Phys. Chem. Solids **28**, 1177 (1967).
[17]S. R. Kurtz, K. Emery, and J. M. Olson, in *Proceedings of the First World Conference on Photovoltaic Energy Conversion, Waikoloa, HI* (IEEE, New York, 1994), p. 1733.
[18]C. R. Osterwald, K. A. Emery, D. R. Myers, and R. E. Hart, in *Proceedings of the 21st IEEE Photovoltaic Specialists Conference, Kissimmee, FL* (IEEE, New York, 1990), p. 1062.
[19]M. A. Steiner, J. F. Geisz, T. E. Moriarty, R. M. France, W. E. McMahon, J. M. Olson, S. R. Kurtz, and D. J. Friedman, "Measuring IV curves and subcell photocurrents in the presence of luminescent coupling," J. Photovoltaics (submitted).
[20]G. Bader, P. V. Ashrit, F. E. Girouard and V.-V. Truong, Appl. Opt. **34**, 1684 (1995).
[21]A. S. Brown and M. A. Green, in *Proceedings of the 29th IEEE Photovoltaic Specialists Conference, New Orleans, LA* (IEEE, New York, 2002), p. 868.